Supplementary Information for

Early volatile depletion on planetesimals inferred from C-S systematics of iron meteorite parent bodies

Marc M. Hirschmann[1,*], Edwin A. Bergin[2], Geoff A. Blake[3], Fred J. Ciesla[4], Jie Li[5]

[1] Department of Earth and Environmental Sciences, University of Minnesota, Minneapolis, MN 55455.

[2] Department of Astronomy, University of Michigan, Ann Arbor, MI 48109.

[3] Division of Geological & Planetary Sciences, California Institute of Technology, Pasadena, CA 91125.

[4] Department of Geophysical Sciences and Chicago Center for Cosmochemistry, University of Chicago, Chicago, IL 60637.

[5] Department of Earth and Environmental Sciences, University of Michigan, Ann Arbor, MI 48109.

*Corresponding author: M.M. Hirschmann. mmh@umn.edu

This PDF file includes:

       Supplementary text
       Figures S1 to S2
       Tables S1 to S3

Other supplementary materials for this manuscript include the following:

       Excel spreadsheet for the thermodynamic model used to calculate the C content of Fe-C-S alloy liquids from coexisting Fe-Ni-C solid alloy in Table S2 and Figures 2 and S1. File Name: HirschmannPNAS-CFig2+S1Calc.xlsx

Carbon in iron meteorite groups.

We employ C estimates for 8 magmatic iron meteorite groups (Table S2). Carbon in iron meteorites has been evaluated by bulk analyses (1, 2), by point counting or planimetric analysis of polished slabs (3), and by combining microanalysis with modal analysis (4). In one case, Meibom et al. (5) determined bulk C of a suite of IIIAB irons using nuclear reaction analysis. Groups not included in our compilation were omitted simply because either sulfur or carbon estimates are lacking.

In contrast to sulfur, which is hosted chiefly in accessory phases, carbon in iron meteorites is hosted in FeNi alloy as well as graphite and carbide (4). Within magmatic groups, C concentrations do not show evidence of systematic increases or decreases with indices of differentiation, such as Ni content (4). Consequently, C concentrations indicative of a magmatic group can be inferred from a sampling of individual iron meteorites, without consideration of their placement in a fractional crystallization sequence.

The most comprehensive survey of carbon in iron meteorites comes from the 130 bulk compositions determined by combustion analysis (1, 2). These span the range from 0 to 0.45 wt.% C. Unfortunately, the analyses were specifically targeted to portray the composition of meteoritic metal, and were conducted by bulk analysis of sections of material from which visible inclusions were excluded. As described by Moore et al. (2), this approach eliminated most large grains of graphite and carbide evident to the naked eye, but not finer grains occurring interstitially or as inclusions. Consequently, these analyses underestimate C in irons and iron groups with conspicuous C-rich domains, but can be more accurate for those in which accessory carbon minerals are absent or limited to microscopic interstitial phases.

Buchwald (3) provided bulk estimates of carbon in selected irons based on planimetric analyses and point counting of large etched slabs. Perhaps even more valuably, Buchwald (3) also gave detailed petrographic descriptions of hundreds of irons that were then known. These reveal which irons and groups have large segregations of graphite or carbide evident without the aid of microscopy, have C phases observable only on microscopic investigation, or have no discernable C rich accessory phases at all.

Goldstein et al. (4) presented the most comprehensive modern survey of C in iron meteorites, combining SIMS and EPMA analyses and imaging with modal analyses to construct characteristic C estimates for 4 of the 8 iron groups (IIAB, IIIAB, IVA, IVB) included in the present study. The following paragraphs provide a more detailed discussion of these four groups, comparing Goldstein et al.'s estimates with other available constraints. We also describe evidence for C contents of the groups (IC, IIC, IID, SBT) not investigated by Goldstein et al. (4).

IC We estimate the C concentration for the IC group of 0.15 wt.% from the average of point-counted estimates by Buchwald (3) of meteorites Bendego (0.1 wt.%), Chihuaha City (0.15 wt.%), and Santa Rosa (0.19 wt.%).

IIC We estimate the C concentration of the IIC group of 0.019 wt.%, based on the analyses of Bacrubito, Perryville, and Wiley (4). Detailed petrographic examination of these 3 meteorites by Buchwald (3) did not detect any graphite or carbides, suggesting that the combustion analyses are not biased by selective exclusion of C-rich phases, and that the low average concentration is realistic.

IIAB Goldstein et al. (4) estimated a C content of the IIAB group of 0.01 wt.% based on SIMS analysis of a single meteorite, North Chile, and for this sample, most of the C was considered to reside in small (1 mm) graphite inclusions observed petrographically by Buchwald (3). Bulk analyses of 19 IIAB irons (4) are consistent with this estimate (0.008±0.004 wt.%). Roughly half of the petrograpic analyses of IIABs reveal small 10-100 micron segregations of cohenite±graphite, at times attached to mm-sized sulfide grains (3), whereas no petrographically observed C-rich phases are observed in the others. The latter include the intensively examined Sikhote Alin and also Silver Bell, the IIAB for which Moore et al. (2) and Lewis and Moore (1) report their highest C content (0.22 wt.%). It is difficult to say whether the bulk chemical analyses (1, 2) were on samples that selectively avoided these inclusions, but the consistency of their analytical results suggests that this was not a major factor and that the estimate of Goldstein et al. (4) is reasonable.

IID The average C concentration of 3 IIDs (Carbo, Rodeo, Wallapai) analyzed by (1, 2) is 0.03 wt.% which is consistent with the petrographic estimate (also 0.03 wt.%) of IID N'Kandhla by Buchwald (3). Buchwald's petrographic examination of several IIDs (Bridgewater, Brownfield, Needles, Losttown, Mount Ouray, Puquios, Richa, Wallapai) did not reveal any C-rich phases, but microscopic needles of graphite or carbide rosettes were identified in Carbo, Elbogen, and N'Kandhla. We infer that the combustion analyses are not biased by selective exclusion of C-rich phases, and that the average concentration is realistic.

IIIAB. Goldstein et al. (4) estimated average C concentrations for the IIIAB group to be between 0.001 and 0.01 wt.%. The upper end of this range is consistent with combustion analyses of 52 IIIAB irons that average 0.016±0.012 wt.% (1, 2) and with the average of nuclear reaction analyses of 7 IIIAB irons of 0.0065±0.0035 wt.% (5). Significant C-rich heterogeneities are not likely a problem for this group. For example, no C-rich phases have been noted in extensive studies of very large polished slabs of Cape York (3). We therefore take 0.01 wt.% as a reasonable estimate for the IIIAB group.

IVA and IVB The IVA and IVB groups are strongly depleted in moderately volatile elements Ge and Ga (6) and clearly have very low total carbon, yet quantitative estimates differ significantly. Goldstein et al. (4) report 0.0004 wt.% and 0.0003 wt.% C in groups IVA and IVB, respectively, based on examination of one meteorite (Bishop Canyon, Tawallah Valley) from each group. In contrast, average analyses from (1, 2) for IVA and IVB groups are 0.016 and 0.006 wt.% C from 15 and 4 meteorites, respectively. Goldstein et al. (4) suggest that these larger averages are a consequence of small amounts of contamination in the combustion analyses. In the case of the IVA group, C concentrations for the 15 meteorites range from 0.003 to 0.042 wt.% (1, 2), and it is the more C rich meteorites that are

both most responsible for the relatively high average C concentration and least likely to be impacted by contamination. The four IVB irons range from 0.004 to 0.11 wt.% C (1, 2). Also, for the 19 IVA and IVB irons analyzed by combustion, analyses on duplicate aliquots were performed and are reported individually for the 16 that come from the study of Moore et al. (2). Where reported, the duplicates closely reproduced one another. Though it is quite probable that the combustion analyses were inflated slightly from analytical blanks comparable to the lowest reported concentrations for individual analyses (0.003-0.005 wt.% C), these would not be nearly sufficient to account for the differences with the SIMS study of Goldstein et al. (4), at least for the IVA group. Three of the four irons from the IVB group are close to this minimum threshold, but the fourth, Deep Spring, with 0.011 wt.%, is greater. At the same time, the average concentrations derived by Goldstein et al. (4) for groups IVA and IVB come from just 6 analyzed SIMS spots on Bishop Canyon and 4 on Tawallah Valley, and therefore it is possible that local microscopic concentrations of C, averaged into the bulk combustion analyses, were missed by the microanalytical approach. On balance, we believe that the average combustion analyses may be more characteristic of the IVA and possibly the IVB groups, though we also consider the more extremely depleted alternative values from Goldstein et al. (4).

SBT The South Byron Trio is a small grouplet of irons (7, 8). We estimate a C concentration of 0.006 wt.%, based on combustion analysis of South Byron (2). Low estimated C concentrations are consistent with petrographic examination, as both conventional metallography (2), and detailed electron microscopy (8) have not revealed any macroscopic or microscopic C-rich phases.

Partial Degassing of Planetesimal Interiors

Partial degassing of planetesimal interiors without wholesale melting and formation of surface magma oceans is the third differentiation process discussed in the main text and is illustrated in Fig. 4B. It could occur either owing to impacts or to igneous crust formation. Of these, degassing associated with impacts is likely more effective, as it promotes (localized) heating that can induce metamorphic devolatilization over a wide area or high degree partial melting in a more limited domain. In the latter, volatile loss is controlled by magmatic degassing. In contrast, volatile dep;etion from planetesimal interiors by extraction of silicate melt is controlled by partitioning between residual mantle phases and silicate magma. This is comparatively inefficient. For example, under even modestly reduced conditions, the concentration of C in graphite-saturated magmas is severely limited (9, 10), impeding significant C extraction. Solubility of S under reduced conditions can be much greater, up to ~1 wt. % (11), but this will only diminish the S concentration of the residual interior if the initial concentration is less than that of the magma. In such a scenario, S would behave as a mildly incompatible element. But even highly devolatilized chondrites have >1 wt.% S (e.g., 1.5 wt. % S in VDC, Table S1), meaning extraction of a melt with 1 wt.% S would leave behind a mantle with *increased* bulk S concentration.

The partial degassing trends depicted in Fig 4B span a range of behavior from loss of C and full retention of S ($\Delta S=0$, inset to Fig. 4B) to equal loss of S and C ($\Delta S=$

ΔC). These limits were chosen owing to the greater solubility of S relative to C in silicate magmas (Table S3), meaning that degassing should affect C more than S. In the case of igneous extraction of melt from a solid matrix under reducing conditions, the opposite relationship can hold, with retention of C and loss of S. This could lead to increases in C/S with modest changes in C. However, under reduced conditions, the efficacy of this mechanism is limited unless the source is already highly depleted in S. For example, extraction of 20% basalt with negligible C and 1 wt.% S from a VDC planetesimal interior (1.5 wt.% S, 0.022 C/S; Table S1) would produce a residuum (1.6 wt. % S; 0.026 C/S) that was little-changed. Extraction of the same basalt from a much more depleted source could have a larger effect, e.g., if the initial source had 0.01 wt.% C and 0.3 wt.% S, the C/S ratio would go from 0.033 to 0.1.

Vapor loss from iron cores without silicate mantles

One process suggested to account for volatile depletion of some parent body cores is re-melting of preexisting metallic cores that had previously lost their silicate mantles. Pd-Ag isotopes provide evidence for such a process for group IVA (12, 13), which is highly depleted in both C and S (Fig 4; Table S2). However, owing to the large disparity in vapor pressures between S and C above molten iron, it is S, rather than C that would be lost from such a process. For example, at 2000 K, an Fe-S melt with mole fraction of S equal to 0.1 has a S vapor pressure of ~1000 Pa (14), whereas the C vapor pressure of a graphite-saturated iron alloy melt would be eight orders of magnitude lower (10^{-5} Pa; (15)), and an unsaturated melt would have C vapor pressure commensurately lower (with vapor pressures of both elements calculated as monatomic species). Consequently, evaporation of a hot iron mass into a vacuum would deplete residual iron bodies in S and have little effect on their C contents, causing increased C/S at near-constant C (Fig. 4C).

Calculated C partitioning between taenite and Fe-C-S melts

Calculations of partitioning of C between taenite and coexisting alloy melt (Fig. S1) are performed by fixing the solid alloy composition and calculating the activity of C using the model of (16) and then at fixed wt.% S in the liquid, searching iteratively for the C concentration in liquid Fe-C-S that matches that activity, using the model of (17). For both models, C activities are relative to a standard state of unity for graphite saturation. Increased S in the liquid greatly enhances the activity coefficient of C in the liquid, thereby stabilizing C in the solid relative to the liquid. The role of Ni in the liquid is ignored, but because Ni diminishes the concentration of C required to saturate graphite by about 20% (relative) for 20 wt.% Ni (18, 19), its effect would be to increase slightly calculated values of D_C and therefore to decrease the inferred C contents of iron parent body liquids.
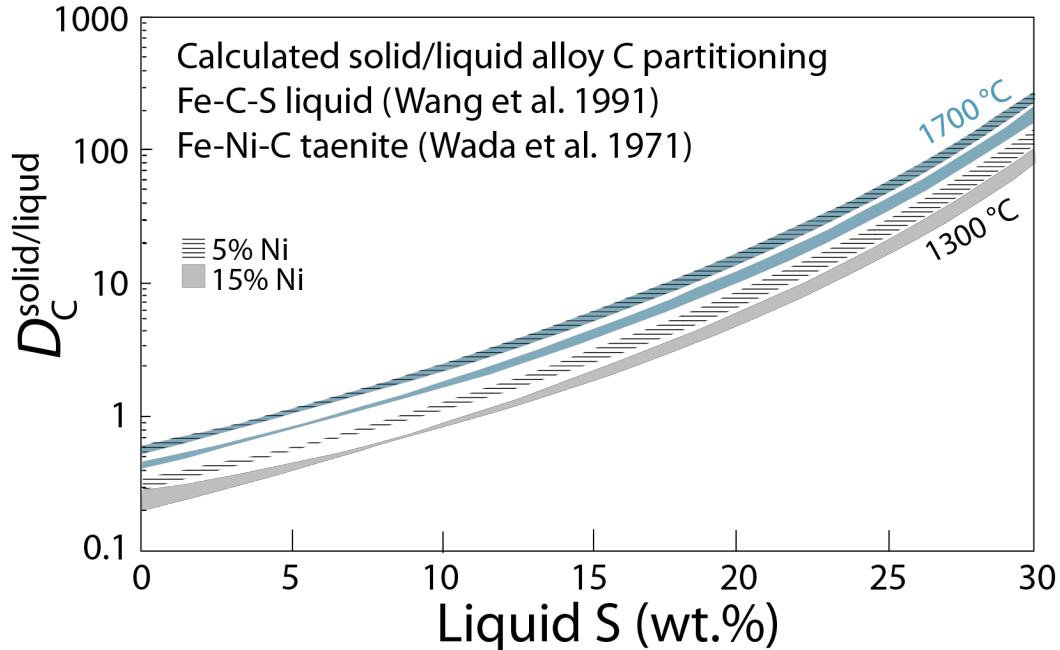
Fig. S1 Calculated partitioning of C between Fe-Ni-C solid taenite (16) and Fe-C-S liquid (17) as a function of liquid S content at 1300 and 1700 °C and 5 and 15 wt.% Ni in the solid. Each band is calculated for solid C concentrations ranging from 0.01 to 0.5 wt.%. For calculations, see Supplementary File HirschmannPNAS-CFig2+S1Calc.xlsx

Estimating bulk C in parent body cores.

The procedure employed in this work to calculate the C of parent body cores assumes that the C concentration of iron meteorites represents that of a pure cumulate taenite, meaning solids precipitated from molten alloy. If these meteorites solidified instead as cumulate taenite combined with some fraction of solidified liquid trapped in the cumulate interstices, this assumption will not be wholly accurate. If that trapped liquid was enriched in C relative to the taenite (D_C < 1, applicable to liquids with less than ~9 wt.% S, Fig. S1, or 12 of the 18 groups shown in Figs. 2-4), then the actual aggregate solid would have had greater C than a pure cumulate, and the calculation would overestimate the parent liquid C content. This is the basis for the statement in the main text that the calculations provide maximum C contents of the iron parent body liquid.

If the trapped liquid had similar C relative to the taenite, as would be the case for parent bodies with liquid S contents 9-12 wt.% (4 of the 18 groups shown in Figs. 2-4), then the applicable D_C would be close to unity and the trapped liquid would have little effect on the calculations. In the case where the trapped liquid was significantly enriched in S, as for the IIAB group if the S content was as inferred by the method of Chabot (20) (17 wt.% S, Fig. 2, Table S2) and the IC group (19 wt.%, Fig. 2, Table S2), then the applicable D_C would be < 1 and the trapped liquid low in C. In this case, the bulk meteorite C content, and the calculated liquid C content could both be underestimates by a maximum factor of (1-F), where F is the fraction of a trapped liquid with negligible C. For example, for the IC group the estimated

6

parent liquid of 0.05 wt.% (Fig. 2) would be revised upward to 0.063 wt.% if the analyzed samples were formed from 80% cumulate taenite and 20% trapped liquid (F=0.2). This difference is small compared to other uncertainties in estimates of C concentrations.

Graphite saturation, alloy unmixing, and ureilite-like planetesimals

As shown in Fig. 4, C-enriched core compositions produced from models of closed system planetesimal differentiation plot within the stability fields of Fe-C-S immiscibility and/or graphite saturation. This occurs for compositions derived from undepleted chondrites, but also for some calculated compositions derived from the depleted VDC planetesimal composition. The possibility of alloy unmixing or graphite saturation during differentiation of primitive parent bodies has several ramifications for planetesimal differentiation.

Fig. S2 shows selected tie-lines of coexisting liquids in the field of unmixing for the system Fe-C-S. (Note that the corresponding immiscibility field for Ni-containing liquid would be smaller, Fig.2). A particular bulk composition plotting along a given curve will unmix to that curve's endpoints. Bulk alloy compositions produced by core segregation of volatile-enriched planetesimals would yield graphite-saturated liquids whereas unmixed liquids formed from less volatile-enriched parents would be graphite-undersaturated.

If bulk alloy compositions derived from volatile-enriched planetesimals unmix, most of the mass becomes a C-rich, S-poor liquid, and a smaller fraction a C-poor, S-rich liquid. This is owing to mass balance, as the bulk composition is closer to the former rather than the latter. The lack of evidence for parent cores similar to such C-rich liquids suggests that volatile-enriched differentiated planetesimals are rare or absent. The less-abundant C-poor conjugate liquids would have > 0.1 wt.% C, which though not highly enriched in C, would be considerably greater C than compositions of medium C/S or low C/S parent body cores (Fig. S2). Such liquids would also be highly enriched (22-35 wt.%) in S. Thus, although unmixing could produce C-poor portions of cores formed from putative volatile-enriched planetesimals, this alone seems an inadequate explanation for inferred iron parent body compositions. Additional volatile-loss processes would be required.

Because all calculated iron parent body compositions plot away from the field of liquid immiscibility (Figs. 2, S2), we infer that bulk parent cores did not originate saturated with respect to a second liquid or graphite, and that early formation of stratified planetesimal cores based on Fe-S-C immiscibility, as suggested previously (21), is unlikely, although disequilibrium layered core segregation (22) cannot be excluded. Also, core segregation could be promoted as liquids evolve to more S-rich differentiates (21, 23, 24), though enrichment in residual liquid Ni inhibits immiscibility (18, 19) (Fig. 2) and could suppress separation of a second liquid.
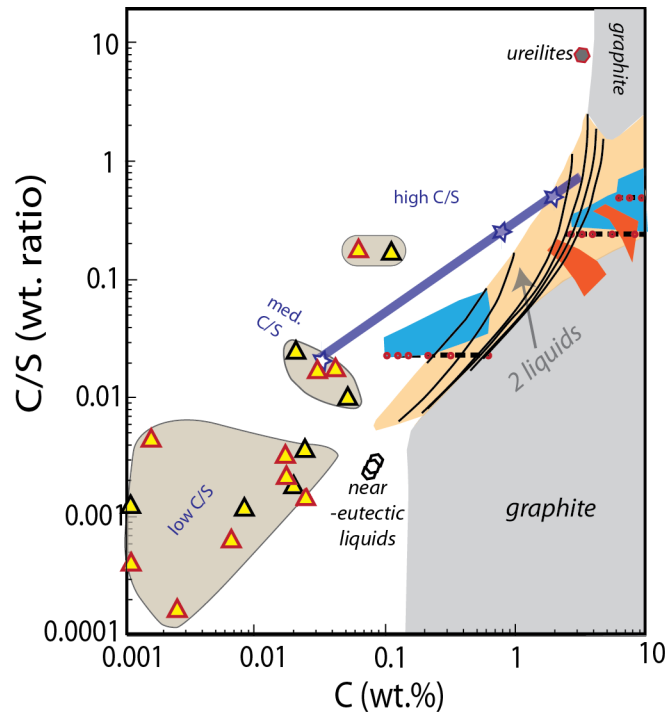
Fig. S2 Calculated liquid alloy compositions formed during core formation of undepleted or less-depleted planetesimals (e.g., VRC, PDC; blue and red shaded regions and black dashed lines are calculated bulk core compositions, for guide see Fig. 4A.), which have bulk compositions within the 2-liquid stability field and will unmix to conjugate C-rich and S-rich liquids, as shown by the black tie lines, calculated from the model of Tafwidli and Kang (25). Tie lines are curved owing to the logarithmic axes. S-rich conjugate liquids have >0.1 wt.% C, and so are more C-enriched than inferred iron meteorite parent bodies. Ureilites (Table S1) are C-rich with high C/S, owing to accumulation of graphitic carbon (26). Polygons marked "near-eutectic liquids" are graphite and iron saturated S-rich melts at 1025-1125°C (27).

Ureilites are ultramafic achondrites that have lost a metal component (26) yet remain markedly enriched in C and poor in S, resulting in super-chondritic C/S (Table S1; Fig. S2). The substantial enrichments in C and C/S seen in ureilites are in some respects complementary to the low C and C/S of many parent body cores, which suggests an alternative scenario for the origin of C-poor planetesimal cores, discussed below. We note that ureilite genesis is known to be quite complex, involving multiple stages and mixing of diverse components (26, 28), and therefore emphasize that this hypothesis applies to bodies with similarities to ureilites – namely an ultramafic silicate planetesimal mantle containing graphite and residual alloy phases – and would not necessarily account for all the features of the actual ureilite parent body

Differentiation of a comparatively volatile-rich planetesimal (similar to the PDC or VRC compositions, Table S1) could lead to formation of two graphite-saturated

liquids, rich in carbon and sulfur respectively. Draining of these liquids could produce a planetesimal core with some similarities to parent cores of iron meteorites, even though the precursor planetesimal was not markedly volatile-depleted, and would leave behind a silicate residue containing graphite and some evidence of residual S-rich and metal rich liquids, as observed in ureilites (29). However, this alternative hypothesis would need to address the challenges noted in the previous paragraphs. Namely, the S-rich liquid produced by unmixing would have > 22 wt. % S and significantly greater C than known parent body cores (Fig. S2). Any contribution of the C-rich conjugate liquid into the accumulated core would dilute the S, but greatly increase the C.

A more extreme version of this hypothesis is formation of metallic cores by extraction of a sulfur-rich liquid near the troilite-alloy eutectic at low temperatures (~1025-1125°C), leaving behind residual iron alloy. (Note that these temperatures are 100-200 °C lower than those inferred to have incited melting and smelting in the ureilite parent body (27, 30)). In graphite-saturated experiments at these conditions, Hayden et al. (27) produced liquids with ~0.08 wt.% C and ~32 wt.% S (Fig. S2). Compared to C-poor immiscible liquids discussed above, these low C contents are closer to inferred iron parent body compositions (Fig. S2), perhaps owing to the lower temperatures, but again, still too C-rich. Also, the S enrichments are extreme compared to those inferred for parent body cores. Finally, such a process would leave most of the highly siderophile elements in residual solid metal, and therefore in the planetesimal mantle, owing to strong solid/liquid partitioning (27). Though these processes are worthy of further investigation, we conclude that the iron meteorites are better explained by devolatilized planetesimals, rather than by retention of C in planetesimal mantles.

Planetesimal core formation calculations

Figure 4 depicts the calculated C and S concentrations of planetesimal cores calculated for four different models. Here we describe the calculations in greater detail, with each model denoted by the labels for the respective cartoons in Fig. 4. For each model, three different beginning planetesimal bulk compositions are considered, as illustrated in Fig.1 and given in Table S1, "VRC" (volatile-rich chondrite), "PDC" (partially devolatilized chondrite), and "VDC" (volatile-depleted chondrite).

Model A1 represents removal of C and S to the core in molten alloy, with no silicate melting, and has been calculated for planetesimals with weight fractions of alloy, x_{alloy}, ranging between 5 and 30%. C and S are assumed to be removed quantitatively from the silicate, resulting in core concentrations that are C_0/x_{alloy}, where C_0 is the concentration of C or S in the original bulk planetesimal.

Model A2 represents removal to the core of C and S from a molten silicate planetesimal interior that has a solid carapace preventing loss of volatiles to the surface or to space. The mass of the solid carapace is assumed to be negligible. The concentration of each element i in the core, C_i^{alloy}, is given by

$$C_i^{alloy} = \frac{C_i^0 D_i^{alloy/silicate} Q}{[(1 - x_{alloy}) + x_{alloy}DQ]} \,,$$ Eqn. S1

where $D_i^{alloy/silicate}$ is the applicable partition coefficient between molten alloy and silicate, and Q is the alloy/silicate equilibration factor (31) ranging from 0 (no chemical equilibrium) to 1 (complete equilibrium). For each planetesimal bulk composition in Fig. 4A, the shaded region represents calculations from Eqn. S1 with values of x_{alloy} ranging from 0.05 up to 0.3 and values of Q ranging from 0.5 to 1. Values of $D^{alloy/silicate}$ depend on oxygen fugacity (f_{O2}) and alloy liquid composition and are given in Table S3.

Model *B* represents removal to the core of C and S from a molten silicate planetesimal interior that has experienced degassing to the surface either prior to or synchronous with metal-silicate equilibration. This calculation occurs in two steps, first volatile loss, followed by core separation, with the latter calculated from Eqn. S1 with an appropriately modified bulk composition. Volatile loss is considered to amount to 0-90% of the original planetesimal carbon, with no sulfur loss ($\Delta S=0$, forming the diagonal trend in the inset to Fig. 4B), carbon and sulfur loss in equal proportions ($\Delta C=\Delta S$, forming the horizontal trend), or intermediate relative losses of carbon and sulfur (forming the shaded area between the diagonal and horizontal trends).

Model *C* represents removal to the core of C and S from an entirely molten planetesimal in which core-forming alloy, molten silicate, and overlying degassed atmosphere equilibrate with one another following the model of Hirschmann (32). The atmosphere exerts vapor pressures on the underlying condensed liquids according to its mass and to planetesimal gravity, which is proportional to planetesimal radius. It is assumed that this atmosphere is later lost to space, but for simplicity, only after separation of alloy to the core. If part of the atmosphere is lost prior to silicate-alloy separation, then the resulting core would be further depleted in C and S owing to enhanced degassing. Partitioning between the three reservoirs, molten core, molten silicate, and atmosphere produces gives the mass fraction of element *i* in the atmosphere, $\dfrac{M_i^{atm}}{M_i}$, as.

$$\frac{M_i^{atm}}{M_i} = \left[\left(\frac{4}{9} G s_i r_i \rho R^2 \right) \left(\left(1 - x_{alloy} \right) + x_{alloy} Q D_i^{alloy/silicate} \right) + 1 \right]^{-1}$$ (Eqn. S2)

(32), where G is the gravitational constant, s_i is the solubility factor specifying the concentration of element *i* dissolved in silicate melt as a function of its partial pressure in the atmosphere (Table S3), ρ is the mean density of the planetesimal (3500 kg/m^3), and R is the planetesimal radius. The parameter r_i is a mass factor that corrects for the difference between the mass of element *i* in the atmosphere and the mass of its gaseous species. Sulfur is assumed to degas as H_2S, and so

r_S=(38/36), and C as CO, giving r_C=(28/12). The corresponding core concentrations are given by

$$C_i^{alloy} = \frac{\left(1 - \dfrac{M_i^{atm}}{M_i}\right) D_i^{alloy/silicate} Q}{[(1 - x_{alloy}) + x_{alloy} DQ]} .$$ (Eqn. S3)

For the calculations shown in Fig. 4C, planetesimal radius is varied from 10 to 500 km, with larger radii resulting in greater retention of volatiles in the core. x^{alloy} is assumed to be 0.2 and Q equal to unity, but resulting core compositions are not strongly sensitive to these assumptions.

Table S1
C and S in Chondrites, Achondrites & Model Compositions

	S (wt.%)	C (wt.%)	C/S	Source
CI1	5.9	3.2	0.54	(33)
CM2	3.3	2.2	0.67	(33)
T. Lake2	3.65	5.81	1.59	(34, 35)
CR2	0.87	2	2.29	(36, 37)
CO3	2	0.45	0.23	(33)
CV3	2.2	0.56	0.25	(33)
CB3	2.19	0.28	0.13	(38)
CK5	1.46	0.07	0.048	(36, 37, 39)
CK6	0.98	0.03	0.034	(38)
Avg. H	0.11	2	0.055	(33)
Avg. LL	0.09	2.2	0.041	(33)
Avg. L	0.12	2.3	0.052	(33)
EH	0.4	5.8	0.069	(33)
EL	0.36	3.3	0.11	(33)
H3	1.90	0.27	0.14	(38)
H4	1.88	0.11	0.06	(38)
H5	1.95	0.08	0.043	(38)
H6	1.84	0.078	0.042	(38)
L3	1.97	0.53	0.27	(38)
L4	2.21	0.20	0.091	(38)
L5	2.02	0.13	0.066	(38)
L6	2.07	0.11	0.055	(38)
LL3	2.27	0.31	0.13	(38)
LL4	1.72	0.04	0.023	(38)
LL5	1.85	0.07	0.038	(38)
LL6	1.76	0.028	0.016	(38)
Ureilites	0.34	3.20	10.4	(40-42)
Winonaites	6.2	0.34	0.056	(38, 40, 43)
Acapulcoites	2.9	0.04	0.014	(43, 44)
Model Compositions				
DVC	1.45	0.032	0.022	
VRC	4	2	0.5	
PDC	3.2	0.8	0.25	

Table S2
Iron Meteorite Parent Body Compositions

	S wt.%	C† wt.%	Liquid C† wt.%	Liquid C/S	
"cc" parents*					
IIC	8	0.019	**0.023**	0.0030	S (45): C: (1, 2)
IIDw	0.7	0.03	**0.11**	0.15	S: (22) C; (1, 2)
IIDcl	6	0.03	**0.051**	0.008	S:(20) (lo S estimate) C: (1, 2)
IIDch	12	0.03	**0.019**	0.00160	S:(20) (hi S estimate) C: (1, 2)
IVBg	1	0.0003	**0.0011**	0.0011	S: (20, 46) C:(4)
IVBm	1	0.006	**0.021**	0.021	S: (20, 46) C:(1, 2)
SBT	7	0.006	**0.0087**	0.0012	S:(7) C: (2)
"nc" parents*					
IC	19	0.15	**0.026**	0.0014	S (47) C: (3)
IIABw	6	0.01	**0.017**	0.0028	S: (48) C: (4)
IIABc	17	0.01	**0.0025**	0.00015	S: (20)) C: (4)
IIIABw	2	0.01	**0.0230**	0.015	S: (49)C: (1, 2, 4, 5)
IIIABc	12	0.01	**0.0064**	0.00054	S: (20) C: (1, 2, 4, 5)
IVAwm	0.4	0.016	**0.061**	0.15	S: (50) C: (1, 2)
IVAclm	3	0.016	**0.043**	0.014	S: (20)(lo estimate) C: (1, 2)
IVAchm	9	0.016	**0.017**	0.0019	S: (20) (hi estimate) C: (1, 2)
IVAwg	0.4	0.0004	**0.0015**	0.0038	S: (50) C: (4)
IVAclg	3	0.0004	**0.0011**	0.00036	S: (20) (lo estimate) C: (4)
IVAchg	9	0.0004	**0.00044**	0.00005	S: (20) (hi estimate) C: (4)

†For C, data in the second column is inferred mean concentration of C in the iron parent body of each group, and data in the second column ("liquid C"), is the thermodynamically calculated composition of the iron parent body core, as described in the text and depicted in Fig. 2. *"cc" and "nc" irons are those with isotopic affinities to carbonaceous and non-carbonaceous chondrites, as defined by (51). For further explanations of C concentrations, see SI Text.

Table S3
Alloy/silicate partition coefficients
and vapor solubility

Conditions	Alloy/silicate Partition coefficient		Solubility Constant	
	$D_i^{alloy/silicate}$		s_i (kg/Pa)	
	Carbon	Sulfur	Carbon	Sulfur
f_{O2}=IW-1	140	35	1 X 10^{-12}	5 X 10^{-9}
f_{O2}=IW-2	550	27	5 X 10^{-13}	5 X 10^{-9}
f_{O2}=IW-3	2200	13	2 X 10^{-13}	5 X 10^{-9}
S-rich	10	100	5 X 10^{-13}	5 X 10^{-9}
Values are applicable to partitioning between ultramafic silicate melt and Fe-C-S melts at oxygen fugacities (f_{O2}) 1, 2, and 3 log units below that defined by the coexistence of iron-wüstite (IW). The fourth set of values is applicable to S-rich (~20 wt.% S) alloy melts (52). All values from Hirschmann (32) except for alloy-silicate partition coefficients for sulfur-rich melts (52).				

Additional References

1.   C. F. Lewis, C. B. Moore, Chemical analysis of thirty-eight iron meteorites. *Meteoritics* **30**, 195-205 (1971).
2.   C. B. Moore, C. F. Lewis, D. Nava, "Superior analyses of iron meteorites" in Meteorite Research*,* P. M. Millman, Ed. (Springer, 1969), vol. 12, pp. 738-748.
3.   V. F. Buchwald (1975) Handbook of Iron Meteorites. Their History Distribution Composition and Structure. (University of California Press), p 1426.
4.   J. I. Goldstein, G. R. Huss, E. R. D. Scott, Ion microprobe analyses of carbon in Fe-Ni metal in iron meteorites and mesosiderites. *Geochimica Et Cosmochimica Acta* **200**, 367-407 (2017).
5.   A. Meibom, K. L. Rasmussen, O. Hansen, P. Hornsoj , N. Rud (1994) Determination of bulk-carbon contents in seven IIIAB iron meteorites. pp 889-890.
6.   J. I. Goldstein, E. R. D. Scott, N. L. Chabot, Iron meteorites: Crystallization, thermal history, parent bodies, and origin. *Chemie Der Erde-Geochemistry* **69**, 293-325 (2009).
7.   C. D. Hilton, K. R. Bermingham, R. J. Walker, T. J. McCoy, Genetics, crystallization sequence, and age of the South Byron Trio iron meteorites: New insights to carbonaceous chondrite (CC) type parent bodies. *Geochimica Et Cosmochimica Acta* **251**, 217-228 (2019).
8.   T. J. McCoy *et al.*, The Milton pallasite and South Byron Trio irons: Evidence for oxidation and core crystallization. *Geochimica Et Cosmochimica Acta* **259**, 358-370 (2019).
9.   M. M. Hirschmann, A. C. Withers, Ventilation of CO_2 from a reduced mantle and consequences for the early Martian greenhouse. *Earth and Planetary Science Letters* **270**, 147-155 (2008).
10.   B. D. Stanley, M. M. Hirschmann, A. C. Withers, Solubility of C-O-H volatiles in graphite-saturated martian basalts. *Geochimica Et Cosmochimica Acta* **129**, 54-76 (2014).
11.   F. Gaillard, B. Scaillet, The sulfur content of volcanic gases on Mars. *Earth and Planetary Science Letters* **279**, 34-43 (2009).
12.   M. Matthes, M. Fischer-Godde, T. S. Kruijer, T. Kleine, Pd-Ag chronometry of IVA iron meteorites and the crystallization and cooling of a protoplanetary core. *Geochimica Et Cosmochimica Acta* **220**, 82-95 (2018).
13.   M. F. Horan, R. W. Carlson, J. Blichert-Toft, Pd-Ag chronology of volatile depletion, crystallization and shock in the Muonionalusta IVA iron meteorite

and implications for its parent body. *Earth and Planetary Science Letters* **351**, 215-222 (2012).

14. P. Waldner, A. D. Pelton, Thermodynamic modeling of the Fe-S system. *Journal of Phase Equilibria and Diffusion* **26**, 23-38 (2005).

15. R. J. Thorn, G. H. Winslow, Vaporization coefficient of graphite and composition of the equilibrium vapor. *Journal of Chemical Physics* **26**, 186-196 (1957).

16. T. Wada, H. Wada, J. F. Elliott, J. Chipman, Thermodynamics of fcc Fe-Ni-C and Ni-C alloys. *Metallurgical Transactions* **2**, 2199-+ (1971).

17. C. Wang, J. Hirama, T. Nagasaka, B. Y. Shiro, Phase equilibria of the liquid Fe-C-S ternary system. *Isij International* **31**, 1292-1299 (1991).

18. Z. Zhang, P. Hastings, A. Von der Handt, M. M. Hirschmann, Experimental determination of carbon solubility in Fe-Ni-S melts. *Geochimica Et Cosmochimica Acta* **225**, 66-79 (2018).

19. L. B. Tsymbulov, L. S. Tsemekhman, Solubility of carbon in sulfide melts of the system Fe-Ni-S. *Russian Journal of Applied Chemistry* **74**, 925-929 (2001).

20. N. L. Chabot, Sulfur contents of the parental metallic cores of magmatic iron meteorites. *Geochimica Et Cosmochimica Acta* **68**, 3607-3618 (2004).

21. A. Corgne, B. J. Wood, Y. W. Fei, C- and S-rich molten alloy immiscibility and core formation of planetesimals. *Geochimica Et Cosmochimica Acta* **72**, 2409-2416 (2008).

22. J. T. Wasson, H. Huber, Compositional trends among IID irons; their possible formation from the P-rich lower magma in a two-layer core. *Geochimica Et Cosmochimica Acta* **70**, 6153-6167 (2006).

23. A. G. Tomkins, E. R. Mare, M. Raveggi, Fe-carbide and Fe-sulfide liquid immiscibility in IAB meteorite, Campo del Cielo: Implications for iron meteorite chemistry and planetesimal core compositions. *Geochimica Et Cosmochimica Acta* **117**, 80-98 (2013).

24. N. L. Chabot, M. J. Drake, Crystallization of magmatic iron meteorites: The effects of phosphorus and liquid immiscibility. *Meteoritics & Planetary Science* **35**, 807-816 (2000).

25. F. Tafwidli, Y. B. Kang, Thermodynamic modeling of Fe-C-S ternary system. *Isij International* **57**, 782-790 (2017).

26. C. A. Goodrich, Ureilites - a critical review. *Meteoritics* **27**, 327-352 (1992).

27. L. A. Hayden, J. A. Van Orman, W. F. McDonough, R. D. Ash, C. A. Goodrich, Trace element partitioning in the Fe-S-C system and its implications for planetary differentiation and the thermal history of ureilites. *Geochimica Et Cosmochimica Acta* **75**, 6570-6583 (2011).

28. K. Rankenburg, M. Humayun, A. D. Brandon, J. S. Herrin, Highly siderophile elements in ureilites. *Geochimica Et Cosmochimica Acta* **72**, 4642-4659 (2008).

29. C. A. Goodrich, R. D. Ash, J. A. Van Orman, K. Domanik, W. F. McDonough, Metallic phases and siderophile elements in main group ureilites: Implications for ureilite petrogenesis. *Geochimica Et Cosmochimica Acta* **112**, 340-373 (2013).

30. S. Singletary, T. L. Grove, Experimental constraints on ureilite petrogenesis. *Geochimica Et Cosmochimica Acta* **70**, 1291-1308 (2006).

31. R. Deguen, M. Landeau, P. Olson, Turbulent metal-silicate mixing, fragmentation, and equilibration in magma oceans. *Earth and Planetary Science Letters* **391**, 274-287 (2014).

32. M. M. Hirschmann, Constraints on the early delivery and fractionation of Earth's major volatiles from C/H, C/N, and C/S ratios. *American Mineralogist* **101**, 540-553 (2016).

33. J. T. Wasson, G. W. Kallemeyn, Compositions of chondrites. *Philosophical Transactions of the Royal Society a-Mathematical Physical and Engineering Sciences* **325**, 535-544 (1988).

34. M. M. Grady, A. B. Verchovsky, I. A. Franchi, I. P. Wright, C. T. Pillinger, Light element geochemistry of the Tagish Lake CI2 chondrite: Comparison with CI1 and CM2 meteorites. *Meteoritics & Planetary Science* **37**, 713-735 (2002).

35. P. G. Brown *et al.*, The fall, recovery, orbit, and composition of the Tagish Lake meteorite: A new type of carbonaceous chondrite. *Science* **290**, 320-325 (2000).

36. V. K. Pearson, M. A. Sephton, I. A. Franchi, J. M. Gibson, I. Gilmour, Carbon and nitrogen in carbonaceous chondrites: Elemental abundances and stable isotopic compositions. *Meteoritics & Planetary Science* **41**, 1899-1918 (2006).

37. N. Braukmuller, F. Wombacher, D. C. Hezel, R. Escoube, C. Munker, The chemical composition of carbonaceous chondrites: Implications for volatile element depletion, complementarity and alteration. *Geochimica Et Cosmochimica Acta* **239**, 17-48 (2018).

38. E. Jarosewich, Chemical analyses of meteorites at the Smithsonian Institution: An update. *Meteoritics & Planetary Science* **41**, 1381-1382 (2006).

39. B. H. Mason, H. B. Wiik, Descriptions of two meteorites: Karoonda and Erakot. *American Museum novitates* **2115** 1-10 (1962).

40. M. M. Grady, I. P. Wright, P. K. Swart, C. T. Pillinger, The carbon and nitrogen isotopic composition of ureilites - implications for their genesis. *Geochimica et Cosmochimica Acta* **49**, 903-915 (1985).

41. H. Downes *et al.*, Isotopic composition of carbon and nitrogen in ureilitic fragments of the Almahata Sitta meteorite. *Meteoritics & Planetary Science* **50**, 255-272 (2015).

42. E. K. Gibson, Nature of carbon and sulfur phases and inorganic gases in Kenna ureilite. *Geochimica Et Cosmochimica Acta* **40**, 1459-1464 (1976).

43. G. Dreibus, H. Palme, B. Spettel, J. Zipfel, H. Wanke, Sulfur and selenium in chondritic meteorites. *Meteoritics* **30**, 439-445 (1995).

44. M. M. Grady, C. T. Pillinger, Carbon isotope relationships in winonaites and forsterite chondrites. *Geochimica Et Cosmochimica Acta* **50**, 255-263 (1986).

45. H. A. Tornabene, C. D. Hilton, K. R. Bermingham, R. D. Ash, R. J. Walker, Genetics, age and crystallization history of group IIC iron meteorites. *Geochimica Et Cosmochimica Acta* **288**, 36-50 (2020).

46. K. L. Rasmussen, D. J. Malvin, V. F. Buchwald, J. T. Wasson, Compositional trends and cooling rates of group-IVB iron-meteorites. *Geochimica Et Cosmochimica Acta* **48**, 805-813 (1984).

47. H. A. Tornabene, R. D. Ash, R. J. Walker (2021) New insights to the genetics, formation, and crystallization history of group IC iron meteorites. in *Lunar and Planetary Science Conference*.

48. J. T. Wasson, H. Huber, D. J. Malvin, Formation of IIAB iron meteorites. *Geochimica Et Cosmochimica Acta* **71**, 760-781 (2007).

49. J. T. Wasson, Trapped melt in IIIAB irons; solid/liquid elemental partitioning during the fractionation of the IIIAB magma. *Geochimica Et Cosmochimica Acta* **63**, 2875-2889 (1999).

50. J. T. Wasson, J. W. Richardson, Fractionation trends among IVA iron meteorites: Contrasts with IIIAB trends. *Geochimica Et Cosmochimica Acta* **65**, 951-970 (2001).

51. T. S. Kruijer, C. Burkhardt, G. Budde, T. Kleine, Age of Jupiter inferred from the distinct genetics and formation times of meteorites. *Proceedings of the National Academy of Sciences of the United States of America* **114**, 6712-6716 (2017).

52. D. S. Grewal *et al.*, The fate of nitrogen during core-mantle separation on Earth. *Geochimica Et Cosmochimica Acta* **251**, 87-115 (2019).